Research Paper
Computational Methods for Differential Equations
http://cmde.tabrizu.ac.ir
Vol. *, No. *, *, pp. 1-18
DOI:10.22034/cmde.2025.68401.3312

Dynamical analysis and exact solutions of generalised Zakharov Kuznetsov equation with composite nonlinearity

Abdur Rahman, Md. Golam Hafez*, and Md. Jahidul Islam

Department of Mathematics, Chittagong University of Engineering & Technology, Chattogram 4349, Bangladesh.

Abstract

This study investigates a generalized Zakharov–Kuznetsov (ZK) equation that incorporates mixed nonlinearity (quadratic and square-root terms), anisotropic dispersion, linear damping, and external periodic forcing. The model is motivated by the need to describe nonlinear wave phenomena in dispersive media, where directional dependence, energy dissipation, and external driving play crucial roles in applications ranging from space plasma physics to laboratory plasma confinement and nonlinear optics. Through a traveling wave reduction, the system is transformed into a second-order nonlinear ODE, enabling comprehensive analysis. The onset of chaotic dynamics is rigorously confirmed using Melnikov's method, establishing conditions for transverse homoclinic intersections. We further extend the new mapping method to derive exact solutions for non-polynomial nonlinearities, overcoming limitations of classical approaches. Additional exact solutions via Jacobi elliptic functions are constructed for the quadratic case, providing a complete spectrum of nonlinear waveforms. Numerical simulations reveal transitions between solitonic behavior, weak chaos, and broadband turbulence across parameter regimes, with direct implications for understanding wave instability and energy transfer in driven dissipative systems. These results provide new insights into the complex dynamics of forced-damped nonlinear systems and represent a significant extension of the classical ZK framework, offering both analytical advances and practical tools for predicting nonlinear wave behavior in physical applications.

Keywords. Dynamical Analysis, Zakharov–Kuznetsov equation with composite nonlinearity, Solitary waves.

2010 Mathematics Subject Classification. 35Cxx, 35Bxx, 35Qxx.

1. Introduction

The Zakharov–Kuznetsov (ZK) equation is a well-established model for describing the evolution of nonlinear waves in diverse field of science and engineering, especially in magnetized plasmas, quantum fluids, and nonlinear optical media [5, 7, 8, 11, 17, 18, 31, 34, 35]. As a multidimensional generalization of the Korteweg–de Vries (KdV) equation, it accounts for both nonlinear and dispersive effects in anisotropic media. While the classical ZK equation with quadratic nonlinearity has been extensively studied, real-world plasma and optical systems often exhibit more complex behaviors, including saturable, root-type, or other non-polynomial nonlinearities, along with energy dissipation and external driving forces. To address this gap, we consider the following generalized ZK equation with mixed nonlinearity, with the composite of damping or drift velocity , and external periodic forcing terms:

$$\frac{\partial V}{\partial t}+\underbrace{(aV+b\sqrt{V})}_{\text{Mixed nonlinearity}}\frac{\partial V}{\partial z}+\sigma\frac{\partial^3 V}{\partial z^3}+\delta\nabla_{\perp}^2\frac{\partial V}{\partial z}=\underbrace{-\gamma\frac{\partial V}{\partial z}+F\sin(\omega t)}_{\text{Damping + Forcing}},\tag{1.1}$$

where $V=V(x,y,z,t)$ is the wave function, and the constants $a,b,\sigma,\delta,\gamma,F,\omega$ are physical parameters. The operator $\nabla_{\perp}^2=\partial^2/\partial x^2+\partial^2/\partial y^2$ represents the transverse Laplacian. The nonlinear term $(aV+b\sqrt{V})\partial V/\partial z$ captures

Received: 30 July 2025; Accepted: 14 April 2026.
∗ Corresponding author. Email: hafez@cuet.ac.bd.

a combination of classical quadratic nonlinearity and a non-polynomial square-root nonlinearity. Such mixed nonlinearities are important in systems where both standard fluid-like and anomalous plasma effects are present. The root-type nonlinearity often arises in superthermal plasma environments, quantum fluids, or systems with nonlocal interactions. This combination allows the equation to describe a richer class of nonlinear wave phenomena, including compact structures and strongly nonlinear solitary waves. The dispersive terms $\sigma\partial^3 V/\partial z^3$ and $\delta\nabla_\perp^2\partial V/\partial z$ account for longitudinal and transverse dispersive effects, respectively. These terms are crucial for the existence of stable waveforms and represent anisotropic dispersion mechanisms typically found in magnetized plasma media. Noted that the inclusion of anisotropic dispersion, linear damping, and external forcing is crucial for enhancing the physical relevance of the model. Anisotropic dispersion captures the directional dependence of wave propagation in stratified fluids, while linear damping accounts for energy dissipation through collisional or viscous effects. External forcing represents continuous energy input from external drivers, such as RF heating in plasmas, which can sustain nonlinear structures against damping or drive the system into chaotic regimes. Together, these elements enable the modeling of realistic non-equilibrium systems where energy input and dissipation compete, leading to rich dynamical behaviors including persistent solitary waves, modulational instabilities, and transition to turbulence. The transverse dispersion, in particular, governs the multidimensional behavior of the wave and is important in extending the one-dimensional KdV-type models to higher-dimensional settings. On the right-hand side, the damping term $-\gamma\partial V/\partial z$ represents energy loss due to collisional dissipation, resistivity, or viscous effects. The external forcing term $F\sin(\omega t)$ introduces a periodic energy input, modeling effects such as electromagnetic pumping, field modulation, or other time-periodic excitations. The interplay between nonlinearity, dispersion, damping, and periodic forcing leads to rich nonlinear dynamics, including soliton excitation, resonance, amplitude modulation, and even chaos under certain regimes. Equation (1.1) reduces to many well-known models under special cases. When $b = \gamma = F = 0$, it recovers the classical Zakharov–Kuznetsov equation [5, 11, 17, 31, 34]. If the transverse term $\delta = 0$, the model simplifies to a one-dimensional KdV-type equation with generalized nonlinearity [1, 2, 25, 28]. In the absence of both dispersive terms ($\sigma = \delta = 0$), it becomes a forced convection–diffusion equation [12, 19, 29]. Thus, the proposed model provides a unified framework for investigating complex nonlinear wave structures in various physical systems such as magnetized plasmas, Bose–Einstein condensates, and nonlinear optical media. However, symbolic calculation methods can also be employed to derive exact analytical solutions efficiently for the evolution equations in understanding the nature of coherent structures propagating in various environments[3, 4, 10, 13, 22].

The main novelty of this work lies in the analytical and dynamical treatment of non-polynomial nonlinearities within the ZK framework. We apply the Melnikov method [9, 16, 23, 27] to rigorously establish the existence of chaotic regimes, marking one of the few applications of this technique to ZK-type models with external forcing. Additionally, we extend the new mapping method (NMM) [26, 32, 33] to derive exact solutions for systems with composite nonlinearities—demonstrating that such equations can admit structured solutions under specific constraint conditions. For the polynomial case, various types of Jacobi elliptic function solutions are also constructed via Jacobi elliptic function method (JEFM) [20].

Complementing the theoretical findings, numerical simulations are used to visualize phase portraits, chaotic attractors, whereas the wave structures are visualized based on our determined analytical solutions under varying parametric regimes. These results reveal transitions between integrable-like behavior, weak chaos, and strong turbulence, offering new insights into nonlinear wave phenomena in physically relevant settings.

2. Derivation of the ODE and formation PDS with external forcing

We assume a solution of the form:

$$V(x, y, z, t) = U(\xi), \quad \xi = lx + my + nz - Mt, \tag{2.1}$$

where l, m, AND n are directional wave numbers which depends on the obliqueness and satisfy $l^2 + m^2 + n^2 = 1$ and M is the wave speed. Substituting Eq. (2.1) into Eq. (1.1) gives

$$-M\frac{dU}{d\xi} + (aU + b\sqrt{U})n\frac{dU}{d\xi} + \sigma n^3\frac{d^3U}{d\xi^3} + \delta(l^2 + m^2)n\frac{d^3U}{d\xi^3} = -\gamma n\frac{dU}{d\xi} + F\sin(\omega t). \tag{2.2}$$

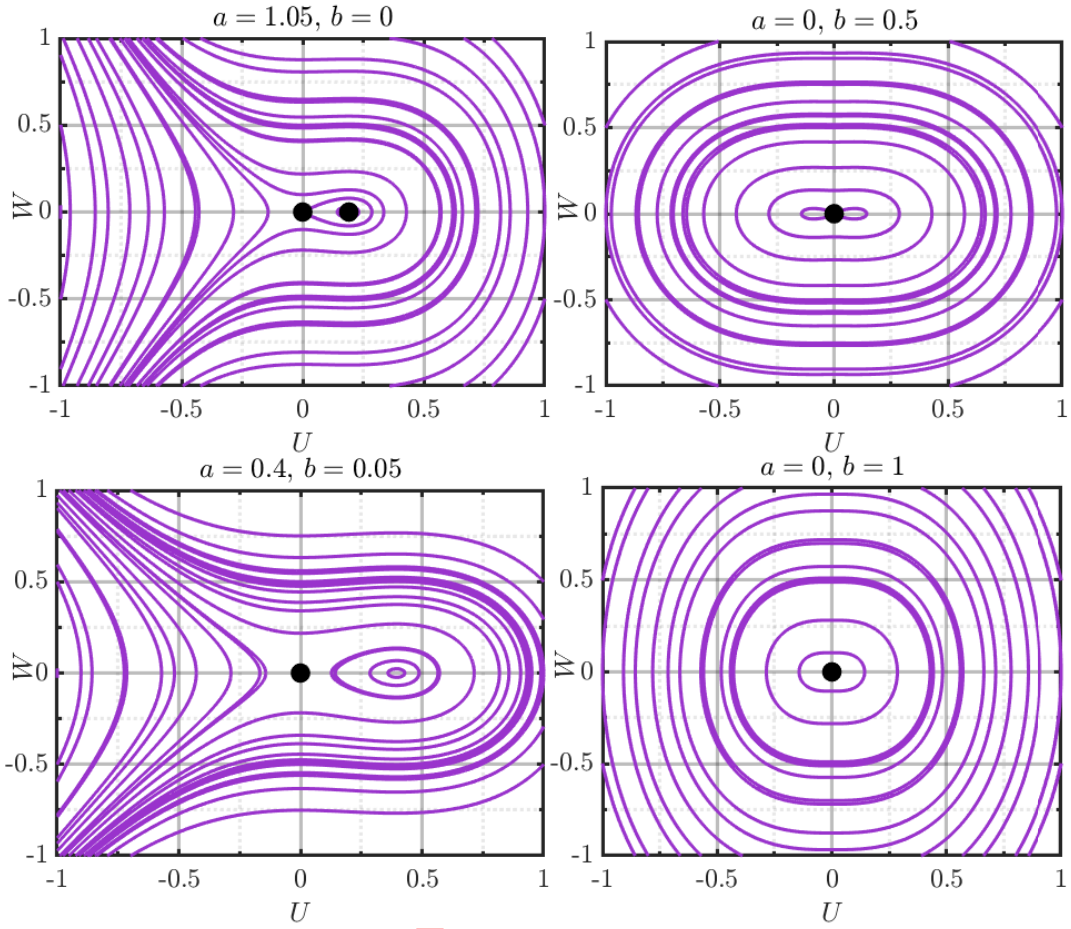

FIGURE 1. Phase portrait of the unperturbed ZK system with $M = 0.1, \sigma = 0.2, \delta = 0.1, \theta = \pi/15$.

Integrating once with respect to ξ:

$$-MU + \frac{na}{2}U^2 + \frac{2nb}{3}U^{3/2} + D\frac{d^2U}{d\xi^2} = -\gamma nU + F\int \sin(\omega t)d\xi + C, \tag{2.3}$$

where C is an integration constant (set to zero for localized solutions) and $D = \sigma n^3 + \delta(l^2 + m^2)n \implies D = \sigma n^3 + \delta(1-n^2)n$, where $n = \cos(\theta)$ and θ is the obliqueness. To from PDS, one needs to use forcing term transformation. Hence, approximating $t \approx -\xi/M$, one obtains $\sin(\omega t) \approx \sin\left(-\frac{\omega\xi}{M}\right) = -\sin\left(\frac{\omega\xi}{M}\right)$, and $\int \sin(\omega t)d\xi \approx \frac{M}{\omega}\cos\left(\frac{\omega\xi}{M}\right)$. By introducing small parameter ϵ, that is $\gamma \to \epsilon\gamma, \quad F \to \epsilon F$, the following ODE is obtained:

$$\frac{d^2U}{d\xi^2} = \frac{1}{D}\left(MU - \frac{na}{2}U^2 - \frac{2nb}{3}U^{3/2}\right) + \epsilon\frac{1}{D}\left(-\gamma nU + \frac{FM}{\omega}\cos\left(\left(\frac{\omega\xi}{M}\right) + \phi_0\right)\right), \tag{2.4}$$

where ϕ_0 is the effective phase shift. This ODE is now suitable for analysis using perturbation methods like Melnikov's method to study chaotic dynamics or soliton stability under damping and forcing. We convert this to a first-order

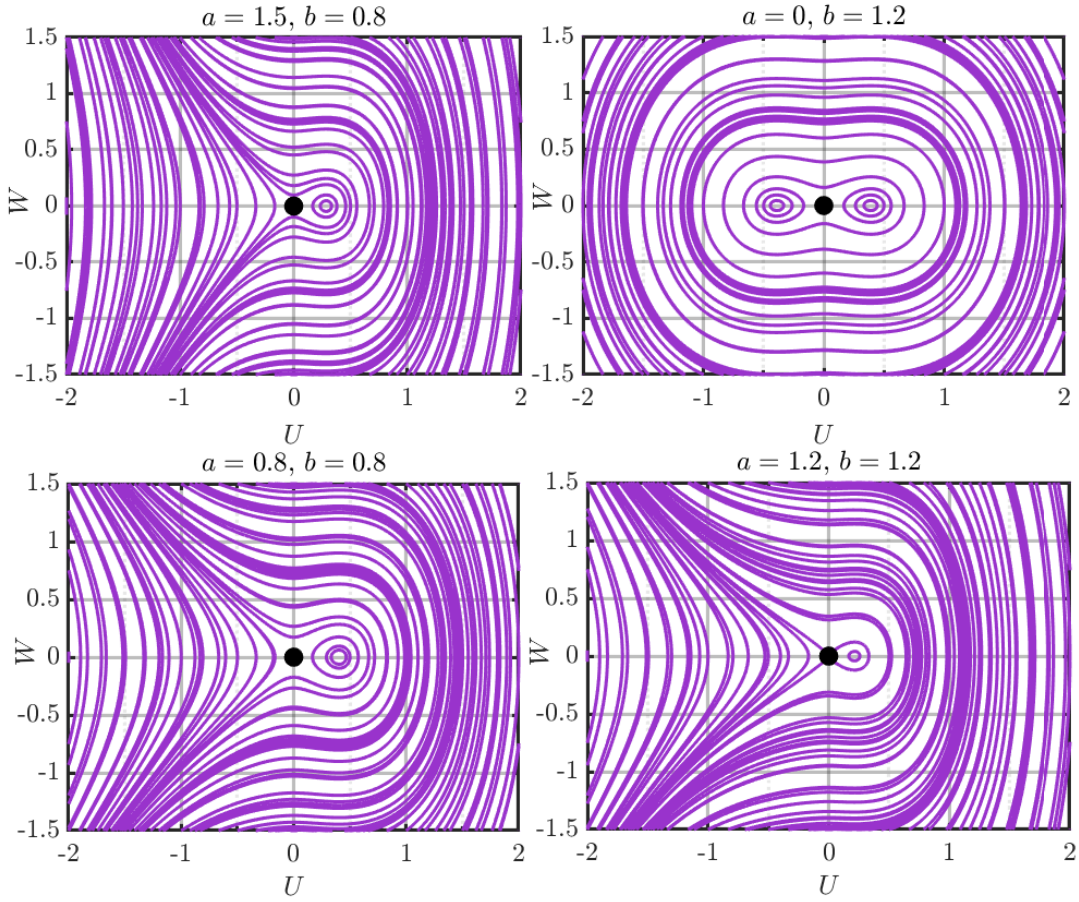

FIGURE 2. Phase portrait of the unperturbed ZK system with $M = 0.5, \sigma = 0.5, \delta = 0.3, \theta = \pi/6$.

system by introducing variables $W = \frac{dU}{d\xi}$ and $\Theta = \frac{\omega\xi}{M} + \phi_0$. The resulting 3D PDS is:

$$\begin{cases} \dfrac{dU}{d\xi} = W, \\ \dfrac{dW}{d\xi} = \dfrac{1}{D}\left(MU - \dfrac{na}{2}U^2 - \dfrac{2nb}{3}U^{3/2}\right) + \epsilon\dfrac{1}{D}\left(-\gamma nU + \dfrac{FM}{\omega}\cos\Theta\right), \\ \dfrac{d\Theta}{d\xi} = \dfrac{\omega}{M}. \end{cases} \tag{2.5}$$

With the absence of damped forcing term, it can be converted to the following 2D PDS:

$$\begin{cases} \dfrac{dU}{d\xi} = W, \\ \dfrac{dW}{d\xi} = \dfrac{1}{D}\left(MU - \dfrac{na}{2}U^2 - \dfrac{2nb}{3}U^{3/2}\right). \end{cases} \tag{2.6}$$

3. Dynamical analysis

Dynamical analysis is essential for understanding the behavior of nonlinear systems. It helps identify equilibrium states, stability, bifurcations, and the onset of chaos, offering deep insights without needing exact solutions. This is

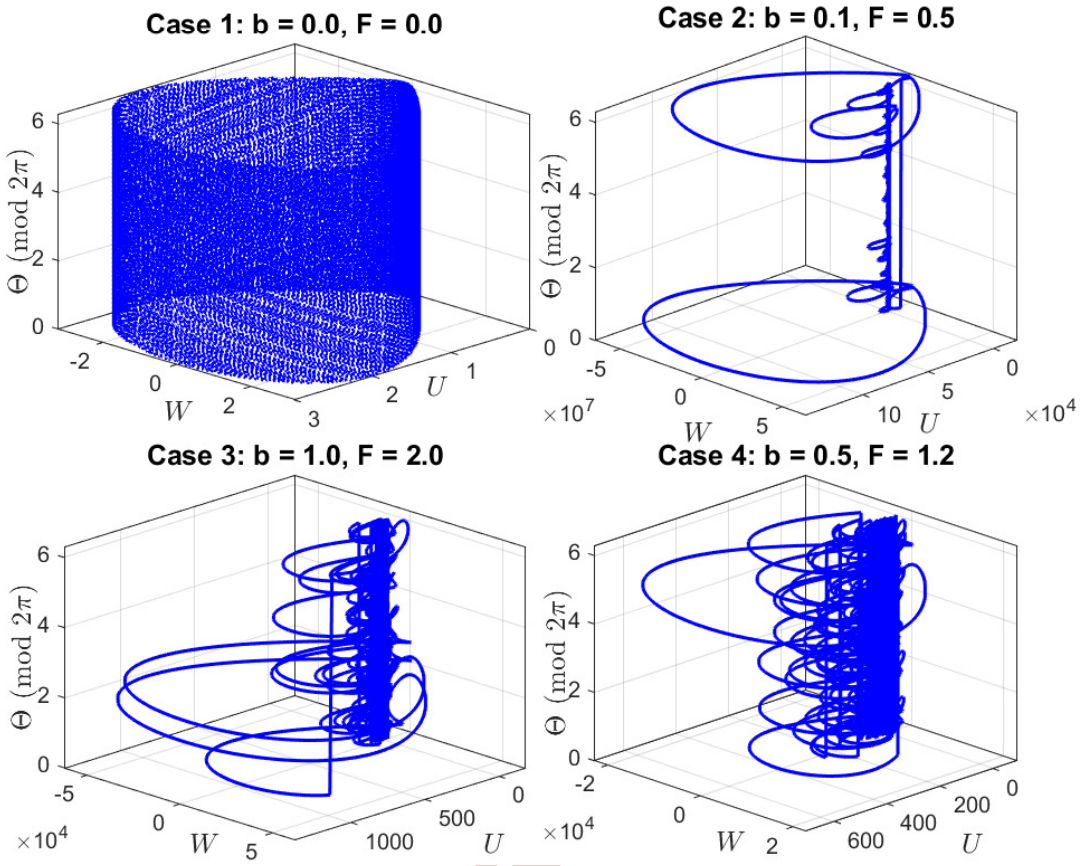

FIGURE 3. 3D phase space trajectory of the perturbed ZK system projected in $(U, W, \Theta \bmod 2\pi)$ space for $a = 1, M = 0.5, \sigma = 0.2, \delta = 0.1, \theta = \pi/3, \gamma = 0.1, \epsilon = 0.1, \omega = 0.1$.

vital in modeling wave dynamics, plasma behavior, and other complex physical systems [6, 14, 15, 21, 30]. To analysis the dynamical features of Eq. (2.6), the following jacobian matrix is formed:

$$J(U,W) = \begin{bmatrix} 0 & 1 \\ \frac{1}{D}\left(M - naU - nb\sqrt{U}\right) & 0 \end{bmatrix}. \tag{3.1}$$

Theorem 3.1 (Stability at the Origin)**.** *For the equilibrium point* $(0,0)$ *of system as in Eq. (2.6):*

(1) *When* $M/D > 0$*, the origin is a saddle point.*
(2) *When* $M/D < 0$*, the origin is a center.*
(3) *When* $M = 0$*, the origin is linearly degenerate.*

Proof. At $(0,0)$, the Jacobian simplifies to:

$$J(0,0) = \begin{bmatrix} 0 & 1 \\ M/D & 0 \end{bmatrix},$$

with characteristic equation $\lambda^2 - M/D = 0$, yielding the stability conditions. □

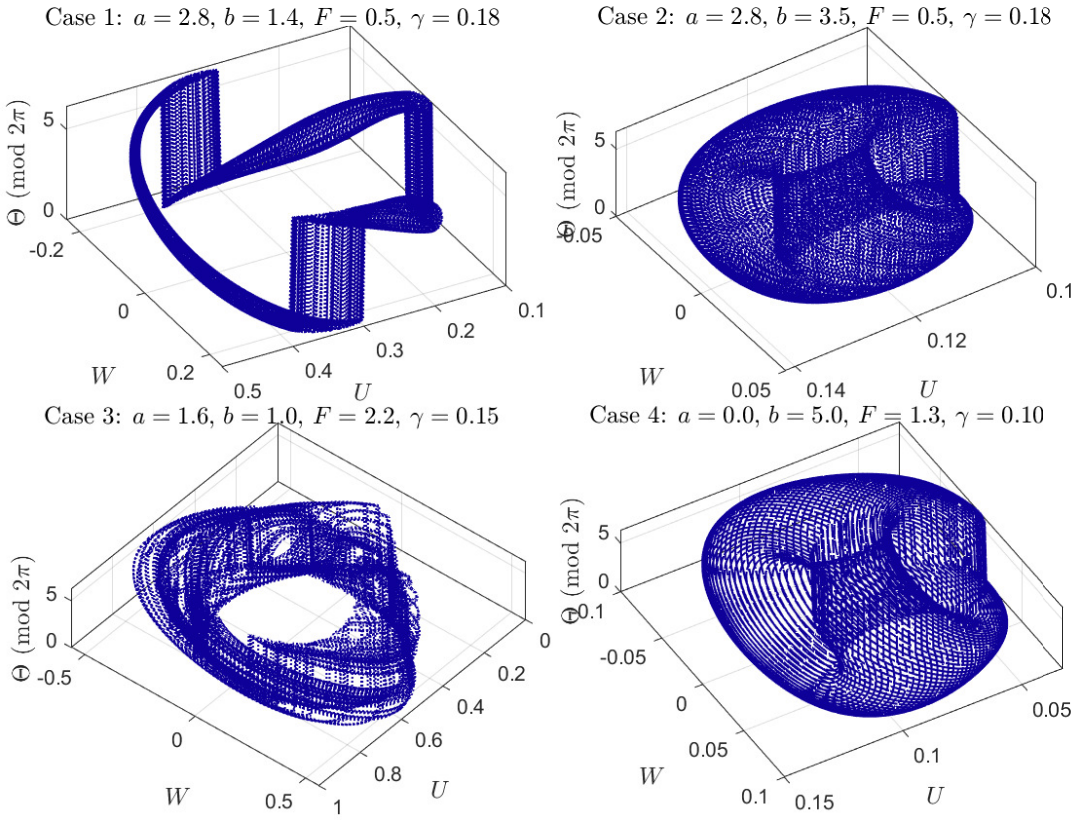

FIGURE 4. 3D phase space trajectory of the perturbed ZK system projected in $(U, W, \Theta \bmod 2\pi)$ space for $M = 0.5, \sigma = 0.6, \delta = 0.3, \theta = \pi/3, \epsilon = 0.1, \omega = 1.8$.

For the case of pure square-root nonlinearity ($a = 0$), additional equilibria occur at:

$$U = \left(\frac{3M}{2nb}\right)^2 =: U_*,$$

where the Jacobian takes the form:

$$J(U_*, 0) = \begin{bmatrix} 0 & 1 \\ -M/(2D) & 0 \end{bmatrix}.$$

In the case of quadratic nonlinearity ($b = 0$), non-trivial equilibria appear at: $U = (2M/na)$, with corresponding Jacobian eigenvalues $\lambda = \pm\sqrt{-M/D}$. However, one can determine the cubic equation as $3naU^3 - 6MU + 4nb = 0$ when $a \neq 0$ and $b \neq 0$. By depending on the parametric values of the parameters, one can determine several real or complex equilibrium points.

Figures 1 and 2 display the phase portraits diagrams under various conditions with the constant values of the remaining parameters. The phase portraits reveal how the interplay between polynomial and root-type nonlinearities profoundly shapes the dynamics of the reduced system. When the system is governed by pure polynomial nonlinearity ($a \neq 0, b = 0$), symmetric phase space structures and closed orbits around a center are observed, with the emergence of a well-defined homoclinic orbit connecting a saddle point. In contrast, when only root-type nonlinearity is present ($a = 0, b \neq 0$), the phase space becomes asymmetric, with the homoclinic loop skewed and saddle points shifted, indicating the softening or hardening nature of the wave response. For mixed nonlinearity ($a, b \neq 0$), the system exhibits richer topological features, including multiple equilibrium points and complex orbit families, suggesting the

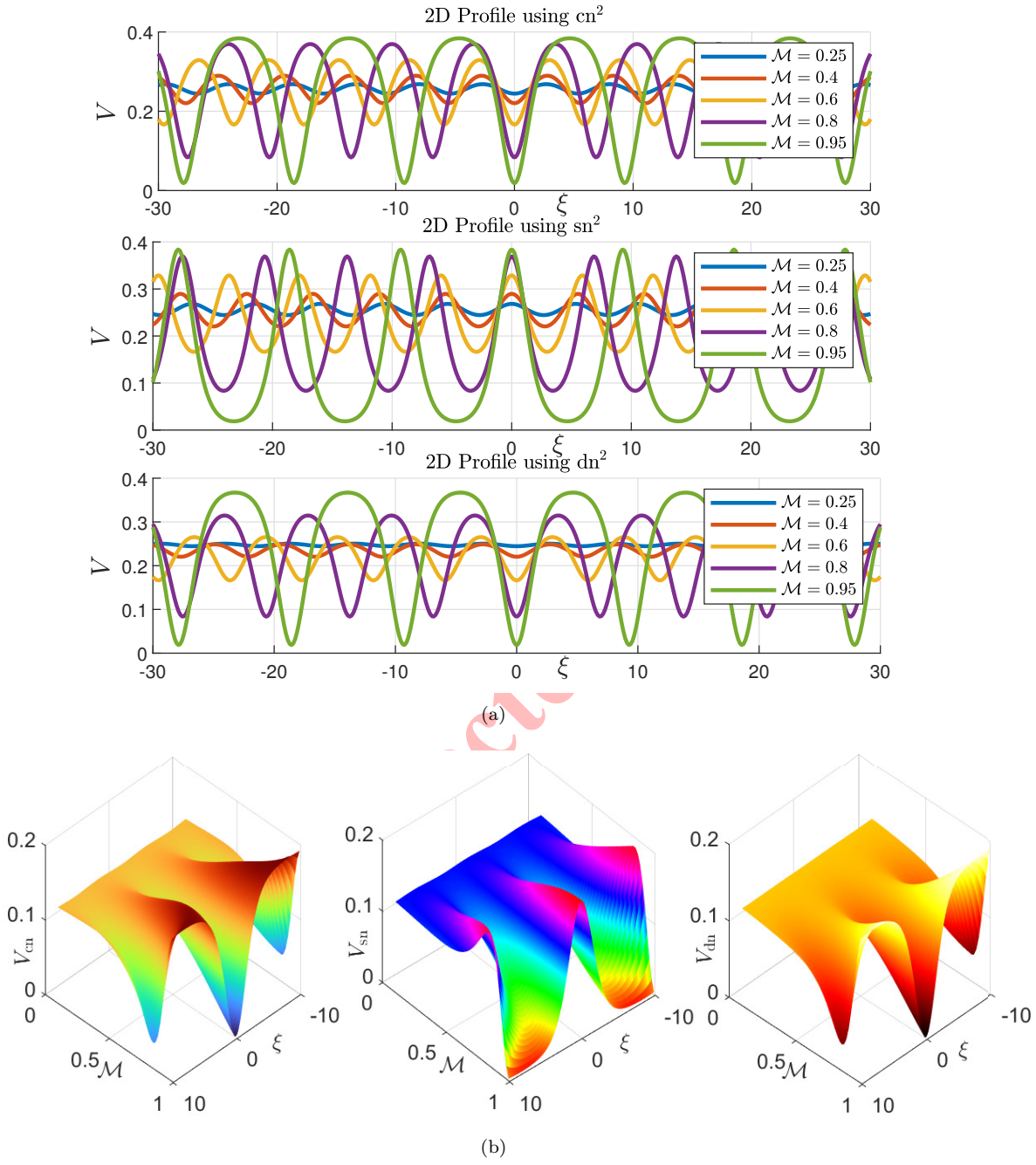

FIGURE 5. Variation of amplitude of the solution of Eq. (1.1). (a) 2D profile of V, and (b) 3D representation of V in terms of elliptic functions cn, sn, and dn, denoted by $V_{\rm cn}$, $V_{\rm sn}$, and $V_{\rm dn}$, respectively, with respect to the stretching coordinate ξ. The plots are shown for $\mathcal{M} \in [0, 1]$ under the parametric values $a = 0.8$, $M = 0.1$, $\sigma = 0.1$, $\delta = 0.4$, and $n = \cos(\pi/6)$.

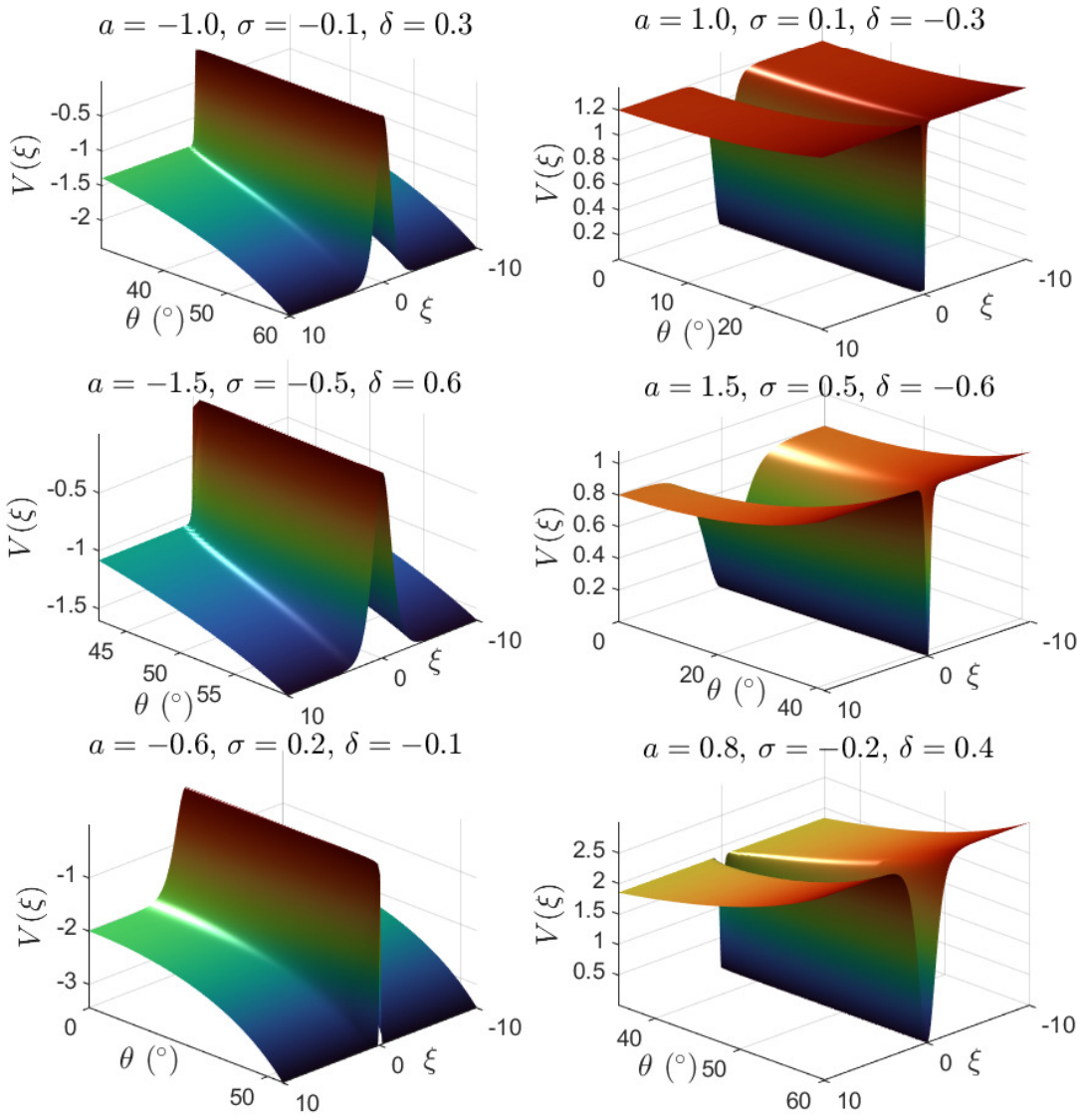

FIGURE 6. 3D surface bright (left column) and dark (rght column) soliton profiles of V with regards to ξ and θ using cn with $\mathcal{M} = 1$ with $M = 0.4$.

coexistence of solitary wave and chaotic structures. Physically, the existence of homoclinic orbits corresponds to solitary wave solutions localized in space, while their deformation or bifurcation indicates the onset of complex wave interactions or instability. By varying the dispersion parameters σ and δ, the number and location of equilibria can be tuned, illustrating the sensitive dependence of nonlinear wave propagation on both the nonlinearity type and dispersive strength in obliquely propagating plasma or fluid media. Now, to check the existence of chaos, the Melnikov's method is implemented:

Theorem 3.2 (Existence of Chaos via Melnikov's Method)**.** *Consider the perturbed ZK system as in Eq. (2.4) where $\epsilon \ll 1$ is a small perturbation parameter, and ϕ_0 is a phase shift. Assume that the unperturbed system ($\epsilon = 0$) admits a homoclinic orbit $U_h(\xi)$ connecting the saddle point at $U = 0$. Then the Melnikov function for transverse intersections*

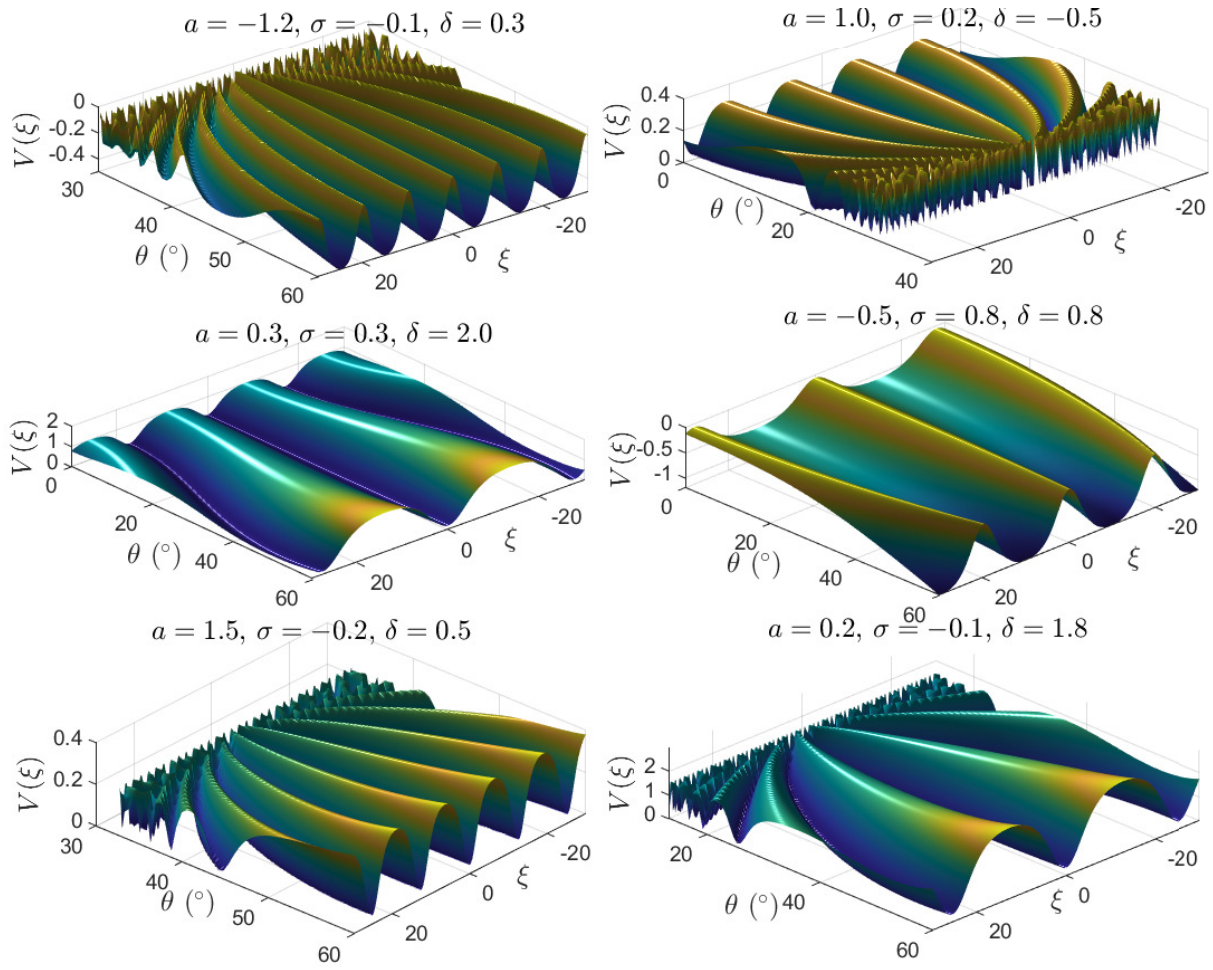

FIGURE 7. Effect of obliqueness on the amplitude of super-nonlinear periodic wave structures that is $V(\xi)$ governed by elliptic function solutions with modulus $\mathcal{M} = 0.9$ and $M = 0.1$. $V(\xi)$ is plotted for six representative parameter sets (a, σ, δ): (a) Dark-type wave for $(-1.2, -0.1, 0.3)$, (b) Bright peak for $(1.0, 0.2, -0.5)$, (c) Upstanding sharp pulse for $(0.3, 0.3, 2.0)$, (d) Broad valley for $(-0.5, 0.8, 0.8)$, (e) Smooth elevation for $(1.5, -0.2, 0.5)$, and (f) Hybrid sharp structure for $(0.2, -0.1, 1.8)$. .

of stable and unstable manifolds is given by:

$$\mathcal{M}(\xi_0) = \int_{-\infty}^{\infty} \left(\frac{dU_h}{d\xi}\right) \left[-\gamma n U_h + \frac{FM}{\omega} \cos\left(\frac{\omega(\xi + \xi_0)}{M} + \phi_0\right)\right] d\xi, \tag{3.2}$$

where ξ_0 is a phase shift parameter along the homoclinic orbit. If there exists $\xi_0^* \in \mathbb{R}$ such that

$$\mathcal{M}(\xi_0^*) = 0 \quad \textit{and} \quad \left.\frac{d\mathcal{M}}{d\xi_0}\right|_{\xi_0 = \xi_0^*} \neq 0,$$

then for $0 < \epsilon \ll 1$, the system exhibits chaotic dynamics through the formation of Smale horseshoes.

Proof. **Step 1: Unperturbed dynamics.** The unperturbed system ($\epsilon = 0$) is Hamiltonian, with

$$W = \frac{dU}{d\xi}, \quad H(U, W) = \frac{1}{2}W^2 - \left(\frac{M}{2D}U^2 - \frac{na}{6D}U^3 - \frac{4nb}{15D}U^{5/2}\right), \tag{3.3}$$

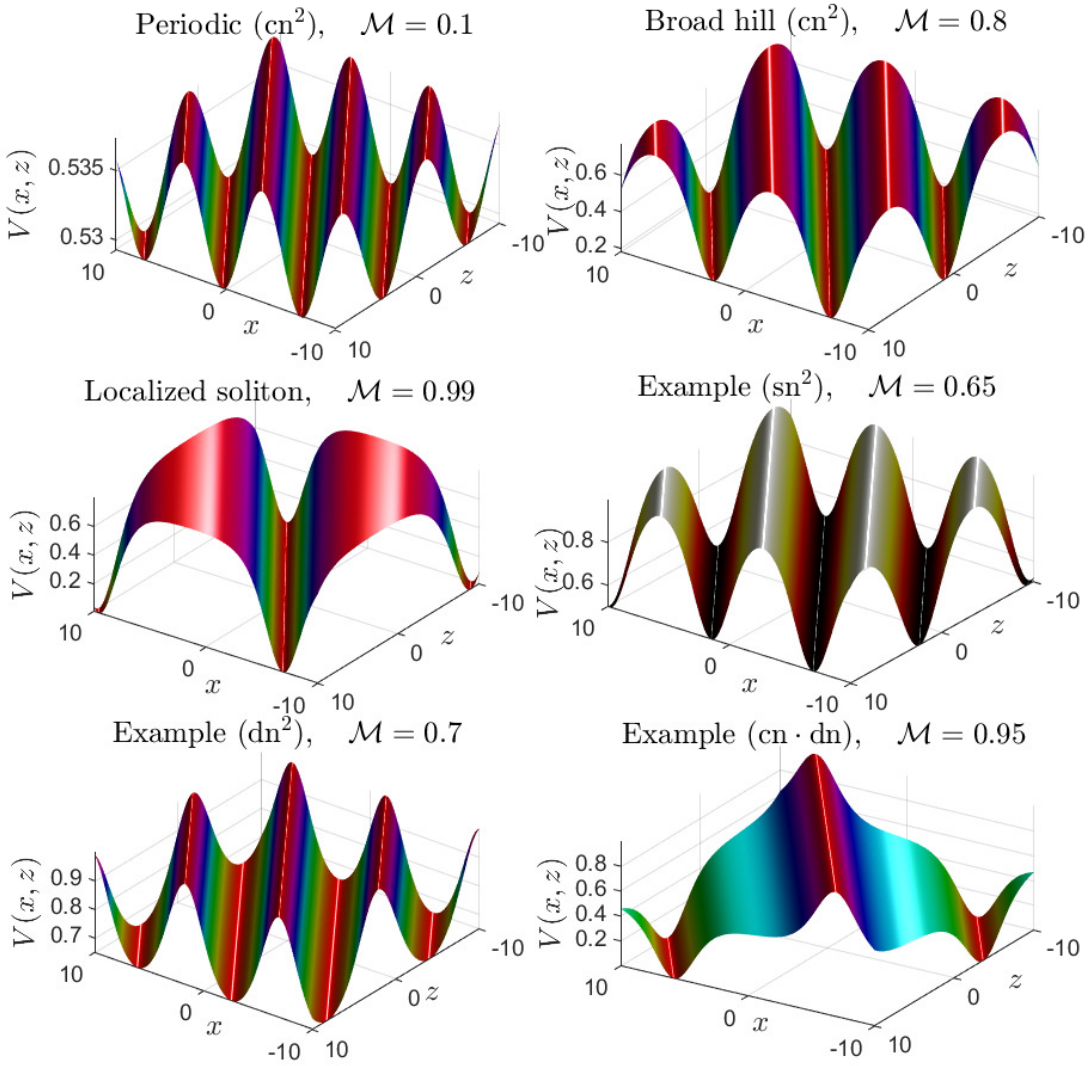

FIGURE 8. Surface plots of nonlinear wave structures $V(x, z)$ with $y = 0$, fixed time 0.5 $\sigma = 0.1$, $\delta = 0.3$, $a = 1.5$, $M = 0.2$ $l = cos(\Theta), \Theta = \pi/4$ and $n = cos(\theta), \theta = \pi/3$ derived from Jacobi elliptic functions under oblique wave propagation. Six representative cases are illustrated: (a) Periodic structure based on cn^2 with $\mathcal{M} = 0.10$, (b) Broad hill profile with cn^2 at $\mathcal{M} = 0.80$, (c) Localized soliton-like structure with cn^2 at $\mathcal{M} = 0.99$, (d) Modulated structure from sn^2 with $\mathcal{M} = 0.65$, (e) Profile using dn^2 with $\mathcal{M} = 0.70$, and (f) Mixed-type structure from cn · dn at $\mathcal{M} = 0.95$. .

admitting a homoclinic orbit $(U_h(\xi), W_h(\xi)) \to (0, 0)$ as $\xi \to \pm\infty$. **Step 2: Perturbation dynamics.** The perturbation is introduced through

$$g(U, \xi) = \begin{pmatrix} 0 \\ -\gamma n U + \frac{FM}{\omega} \cos\left(\frac{\omega\xi}{M} + \phi_0\right) \end{pmatrix}. \tag{3.4}$$

Step 3: Melnikov Integral. The Melnikov function measures the distance between stable and unstable manifolds:

$$\begin{aligned}\mathcal{M}(\xi_0) &= \int_{-\infty}^{\infty} \frac{dU_h}{d\xi}\left[-\gamma n U_h + \frac{FM}{\omega}\cos\left(\tfrac{\omega(\xi+\xi_0)}{M}+\phi_0\right)\right] d\xi \\ &= -\gamma n \underbrace{\int_{-\infty}^{\infty} U_h \frac{dU_h}{d\xi} d\xi}_{=0 \text{ (odd integrand)}} + \frac{FM}{\omega}\int_{-\infty}^{\infty} \frac{dU_h}{d\xi}\cos\left(\tfrac{\omega(\xi+\xi_0)}{M}+\phi_0\right) d\xi. \end{aligned} \tag{3.5}$$

Using the identity

$$\cos\left(\tfrac{\omega(\xi+\xi_0)}{M}+\phi_0\right) = \cos\left(\tfrac{\omega\xi_0}{M}+\phi_0\right)\cos\left(\tfrac{\omega\xi}{M}\right) - \sin\left(\tfrac{\omega\xi_0}{M}+\phi_0\right)\sin\left(\tfrac{\omega\xi}{M}\right),$$

we define

$$I_c = \int_{-\infty}^{\infty} \frac{dU_h}{d\xi}\cos\left(\tfrac{\omega\xi}{M}\right) d\xi, \quad I_s = \int_{-\infty}^{\infty} \frac{dU_h}{d\xi}\sin\left(\tfrac{\omega\xi}{M}\right) d\xi, \tag{3.6}$$

and obtain

$$\mathcal{M}(\xi_0) = \frac{FM}{\omega}\left[I_c\cos\left(\tfrac{\omega\xi_0}{M}+\phi_0\right) - I_s\sin\left(\tfrac{\omega\xi_0}{M}+\phi_0\right)\right]. \tag{3.7}$$

Using trigonometric simplification:

$$\mathcal{M}(\xi_0) = \frac{FM}{\omega}\sqrt{I_c^2+I_s^2}\sin\left(\tfrac{\omega\xi_0}{M}+\phi_0+\alpha\right), \quad \alpha = \arctan\left(\tfrac{I_c}{I_s}\right). \tag{3.8}$$

Step 4: Chaotic Condition. The function $\mathcal{M}(\xi_0)$ has simple zeros if $F \neq 0$ and $\sqrt{I_c^2+I_s^2} \neq 0$, implying that the stable and unstable manifolds intersect transversally. Therefore, for small $\epsilon > 0$, the system exhibits chaotic dynamics via Smale horseshoes. □

Remark 3.3. For $b = 0$, the homoclinic solution reduces to the classical KdV soliton:

$$U_h(\xi) = \frac{3M}{na}\operatorname{sech}^2\left(\tfrac{\sqrt{M}}{2\sqrt{D}}\xi\right), \quad \frac{dU_h}{d\xi} = -\frac{6M\sqrt{M}}{na\sqrt{D}}\operatorname{sech}^2\left(\tfrac{\sqrt{M}}{2\sqrt{D}}\xi\right)\tanh\left(\tfrac{\sqrt{M}}{2\sqrt{D}}\xi\right). \tag{3.9}$$

Using Fourier techniques, we find

$$I_c = \frac{12\pi M^{3/2}\omega}{na\sqrt{D}}\operatorname{csch}\left(\tfrac{\pi\sqrt{D}\omega}{M}\right), \quad I_s = 0. \tag{3.10}$$

For $b \neq 0$, the homoclinic orbit must be computed numerically, and the Melnikov integrals are approximated as

$$I_c(\omega) \approx \int_{-L}^{L} \frac{dU_h}{d\xi}\cos\left(\tfrac{\omega\xi}{M}\right) d\xi, \quad L \gg 1. \tag{3.11}$$

Remark 3.4. The threshold value of the forcing amplitude F required for the onset of chaos satisfies

$$F_c(\omega) = \frac{\gamma n\omega}{M}\left|\frac{\int_{-\infty}^{\infty} U_h \frac{dU_h}{d\xi} d\xi}{I_c}\right|. \tag{3.12}$$

Note that if $\int U_h \frac{dU_h}{d\xi} d\xi = 0$ due to symmetry, then any non-zero forcing $F > 0$ may lead to chaotic behavior. Hence, the dynamical regime shows various structures, such as integrable KdV-like solitons ($b/a = 0$), weak chaos onset ($0 < b/a \ll 1$), and strong chaos ($b/a \sim \mathcal{O}(1)$).

To explore the dynamical behavior of the perturbed Zakharov–Kuznetsov system, we analyze the phase space trajectories in the three-dimensional space (U, W, Θ) for various values of the nonlinear parameters a and b, and the external forcing amplitude F. Figure 3 and 4 reveals diverse dynamical regimes based on the strength and type of nonlinearity. For the integrable case ($a \neq 0$, $b = 0$, $F = 0$), the system exhibits smooth, closed orbits corresponding to regular solitary wave dynamics. When a weak square-root nonlinearity is introduced ($a \neq 0$, $b > 0$), along with a small external force, the orbits begin to show slight distortions and sensitivity to initial conditions, indicating

the onset of weak chaos. As the nonlinearity and forcing amplitude are further increased, the system transitions to a fully chaotic regime characterized by irregular, broadband structures in phase space, signifying strong wave turbulence. An intermediate case highlights the gradual deformation of regular orbits into chaotic attractors. These transitions demonstrate that the interplay between quadratic and square-root nonlinearities, together with periodic forcing, profoundly affects the wave dynamics. Physically, such behavior may correspond to modulational instabilities and resonance interactions in dispersive plasmas or fluids, where external excitation leads to energy redistribution and complex wave interactions. The equilibrium points and their bifurcations also evolve depending on the values of δ and σ through the dispersion coefficient $D = \sigma n^3 + \delta n(1 - n^2)$, and suitable choices of parameters reveal cases with up to three distinct equilibrium points, further enriching the system's phase structure.

4. Exact solutions for the case of quadratic nonlinearity via JEFM with discussion

It is observed that Eq. (2.4) is solvable either $a = 0$ or $b = 0$ along with $\epsilon = 0$, otherwise it is a non-integrable equation. By considering $b = 0$ and $\epsilon = 0$, Eq. (2.4) can be written as

$$\frac{1}{2}anU^2 - MU + D\frac{d^2U}{d\xi^2} = 0. \tag{4.1}$$

We assume a solution based on the Jacobi elliptic cosine function $\mathrm{cn}(B\xi, \mathcal{M})$:

$$U(\xi) = a_0 + a_1\,\mathrm{cn}(B\xi, \mathcal{M}) + a_2\,\mathrm{cn}^2(B\xi, \mathcal{M}). \tag{4.2}$$

Substituting $U(\xi)$ into Eq. (4.1), we equate coefficients of like powers of $\mathrm{cn}(B\chi, m)$ to obtain the algebraic equations (ignored for simplicity). Solving the resulting equations, we determine the expression for a_0, a_2, a_3 and B as below.

$$a_0 = \frac{4B^2D\mathcal{M}^2 + 4B^2D + M}{an}, a_1 = 0, a_2 = -\frac{12B^2D\mathcal{M}^2}{an}, B = \frac{\sqrt{D\sqrt{\mathcal{M}^4 - \mathcal{M}^2 + 1}M}}{2D\sqrt{\mathcal{M}^4 - \mathcal{M}^2 + 1}}.$$

Hence the solution of the considered model equation as in Eq. (1.1) with $b = 0$ and without forced-damped term as

$$V(x, y, z, t) = \frac{4B^2D\mathcal{M}^2 + 4B^2D + M}{an} - \frac{12B^2D\mathcal{M}^2}{an}\mathrm{cn}^2(B\xi, \mathcal{M}), \tag{4.3}$$

where $\xi = lx + my + nz - Mt$. It is noted one can also derive similar type of solutions by considering sn or $cn.dn$ instead of cn and $\mathcal{M} \in [0, 1]$.

Depending on the parameter values, the obtained solutions exhibit various types of wave structures. Furthermore, one can analyze the effect of parameters on the amplitude variation by plotting $V(\xi)$. The shapes of the structures can also be visualized by plotting V as a function of two spatial variables while keeping the third one fixed, such as $V(x, y)$ with z constant, $V(x, z)$ with y constant, or $V(y, z)$ with x constant, at a fixed time. To illustrate it, Figures 5–8 display either variation of amplitude of the wave propagation or various types of coherent structures based on the values $\mathcal{M}$. Figure 5 illustrates the evolution of the amplitude of nonlinear wave profiles constructed from squared Jacobi elliptic functions cn^2, sn^2, and dn^2 under varying modulus $\mathcal{M} \in (0.1, 0.99)$ at fixed obliqueness $\theta = \pi/6$. As $\mathcal{M}$ increases, all three waveforms exhibit stronger localization and amplitude enhancement, with cn^2 producing bright-type solitons, sn^2 yielding symmetric dip-like structures, and dn^2 showing hybrid characteristics. These results confirm that the modulus parameter acts as a tuning knob for soliton shape, and that the system supports a rich class of bounded waveforms under elliptic-function ansatz. Figure 6 presents six representative soliton structures with the variation of their amplitudes corresponding to different combinations of the parameters (a, σ, δ), illustrating the impact of obliqueness θ on the amplitudes of nonlinear wave propagation. Each panel captures a distinct waveform behavior—ranging from bright and dark solitons to flat and hybrid-like profiles—emerging from the analytical solution constructed using the Jacobi elliptic function cn^2. The obliqueness influences the effective dispersion $D(\theta) = \sigma\cos^3\theta + \delta(1 - \cos^2\theta)\cos\theta$, leading to diverse solution morphologies. For instance, bright solitons sharpen and intensify with increasing θ, while dark solitons exhibit deeper troughs or suppressed amplitudes depending on $D(\theta)$'s sign and magnitude. Particularly, cases with high absolute values of a and balanced (σ, δ) produce sharply localized structures, whereas low-dispersion settings induce flattened or asymmetric waves. These results emphasize that obliqueness serves as a bifurcation parameter modulating the nonlinear-dispersive balance, thereby offering rich

dynamical regimes and controllable wave features in oblique wave systems governed by elliptic-function-based soliton solutions. Figure 7 illustrates the emergence of the variation of amplitudes of super-nonlinear periodic waveforms governed by the squared Jacobi elliptic function cn^2 for fixed modulus $\mathcal{M} = 0.9$, with varying obliqueness angle θ and six distinct parameter sets (a, σ, δ). The computed structures span dark dips, bright humps, broad valleys, and hybrid sharp forms, emphasizing how nonlinear dispersion and geometric obliqueness jointly shape wave evolution. The profiles become increasingly modulated as θ varies, revealing rich structural diversity, especially under large nonlinear dispersion (e.g., panel 3 and 6). The analytically computed wave number B ensures dynamically consistent elliptic oscillations. Overall, the simulations demonstrate that super-nonlinear periodicity allows tunable control of waveform morphology under combined parametric and directional modulation. Figure 8 presents a collection of 3D nonlinear wave structures in the (x, z)-plane under fixed obliqueness $\theta = \pi/3$ and directional projection $\Theta = \pi/4$, demonstrating how distinct elliptic-function waveforms evolve in space at a fixed time slice ($t = 0.5$). The profiles span a range of elliptic modulus values $\mathcal{M}$ and functional forms, including cn^2, sn^2, dn^2, and the product $\mathrm{cn} \cdot \mathrm{dn}$. For lower $\mathcal{M}$ (e.g., $\mathcal{M} = 0.1$), the solution appears periodic and wavy, while higher values (e.g., $\mathcal{M} = 0.99$) induce strong localization resembling soliton peaks. Directional cosines ensure proper oblique propagation geometry through $\xi = lx + my + nz - Mt$. Notably, only the cn^2 case uses a fully analytic expression, whereas others are scaled visualizations. These results verify the geometric tunability of nonlinear periodic and solitary structures through combined control of modulus, functional form, and wave obliqueness.

5. Exact solutions for the case of non-polynomial nonlinearity via the extended NMM with discussion

Eq. (2.4) can be written with the presence of non-polynomial nonlinearity by considering $U(\xi) = (\mathcal{U}(\xi))^4$ with $a = 0$, and $\epsilon = 0$ as

$$\left(\frac{d\mathcal{U}}{d\xi}\right)^2 + \frac{1}{3}\mathcal{U}\frac{d^2\mathcal{U}}{d\xi^2} + K_2\mathcal{U}^4 - MK_3\mathcal{U}^2 = 0, \tag{5.1}$$

where $K_2 = (nb)/(18D)$ and $K_3 = 1/(12D)$. Firstly, we need to homogenous balance between higher-order derivative and nonlinearity, which yields $(1 + 1)N + 2 = 4N \implies N = 1$. Thus the NMM suggest that the analytical solution of Eq. (5.1) can be defined as

$$\mathcal{U}(\xi) = \sum_{r=0}^{2N} \mathcal{A}_i(\Psi(\xi))^r, N = 1, \tag{5.2}$$

where $\Psi(\xi)$ satisfy the following the nonlinear ordinary differential equation:

$$\left(\frac{d\Psi(\xi)}{d\xi}\right)^2 = p\Psi(\xi)^2 + \frac{1}{2}q\Psi(\xi)^4 + \frac{1}{3}s\Psi(\xi)^6 + r. \tag{5.3}$$

The above equations yields a huge amount of solutions based on various constrains conditions that are given in Ref. [26, 33]. By substituting Eq. (5.2) along with the consideration of Eq. (5.3), Eq. (5.1) can be converted with grouping terms by powers of Ψ to

$$\begin{aligned}
&\frac{20}{9}\mathcal{A}_2^2 s + K_2\mathcal{A}_2^4 = 0,\\
&\frac{23}{9}\mathcal{A}_1 s\mathcal{A}_2 + 4K_2\mathcal{A}_1\mathcal{A}_2^3 = 0,\\
&\frac{8}{9}\mathcal{A}_2 s\mathcal{A}_0 + 4K_2\mathcal{A}_0\mathcal{A}_2^3 + 3\mathcal{A}_2^2 q + \frac{2}{3}\mathcal{A}_1^2 s + 6K_2\mathcal{A}_1^2\mathcal{A}_2^2 = 0,\\
&\frac{10}{3}\mathcal{A}_1 q\mathcal{A}_2 + \frac{1}{3}\mathcal{A}_1 s\mathcal{A}_0 + 12K_2\mathcal{A}_0\mathcal{A}_1\mathcal{A}_2^2 + 4K_2\mathcal{A}_1^3\mathcal{A}_2 = 0,\\
&12K_2\mathcal{A}_0\mathcal{A}_1^2\mathcal{A}_2 + \mathcal{A}_2 q\mathcal{A}_0 + K_2\mathcal{A}_1^4 + 6K_2\mathcal{A}_0^2\mathcal{A}_2^2 - K_3 M\mathcal{A}_2^2 + \frac{5}{6}\mathcal{A}_1^2 q + \frac{16}{3}\mathcal{A}_2^2 p = 0,
\end{aligned}$$

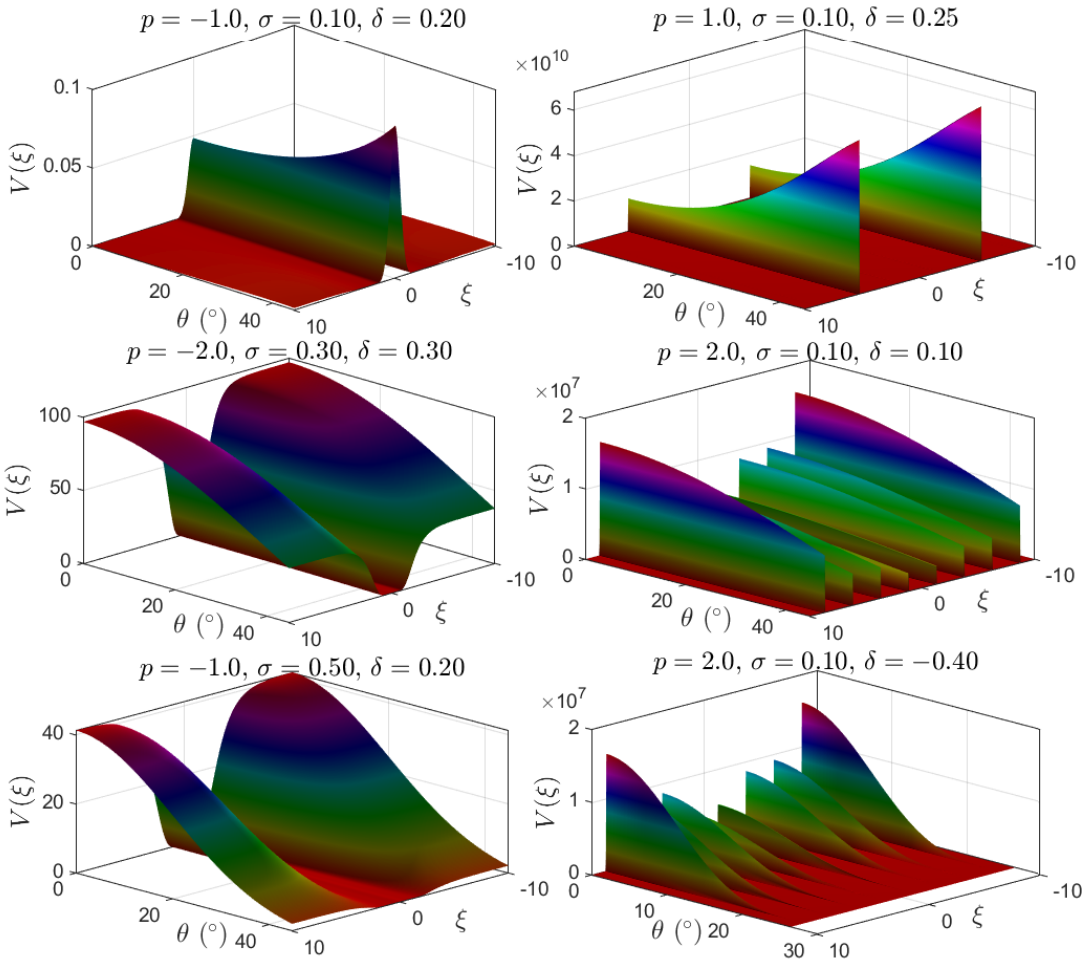

FIGURE 9. Variation of amplitude of non-polynomial wave structures with regards to obliqueness derived from a newly obtained analytical solution to the generalized Zakharov–Kuznetsov (ZK) system with square-root and quartic nonlinearities. The profiles $V(\xi)$ are visualized for six representative cases. Depending on the sign and magnitude of p, the system supports a diverse range of localized waveforms, including: smooth dark soliton-like structures, sharp upstanding peaks, strong nonlinear dark dips, high-intensity spikes, broad humps, and hybrid sharply profiles, respectively.

$$-2K_3M\mathcal{A}_1\mathcal{A}_2+\frac{17}{3}\mathcal{A}_1p\mathcal{A}_2+\frac{1}{3}\mathcal{A}_1q\mathcal{A}_0+4K_2\mathcal{A}_0\mathcal{A}_1^3+12K_2\mathcal{A}_0^2\mathcal{A}_1\mathcal{A}_2=0,$$
$$4K_2\mathcal{A}_0^3\mathcal{A}_2-2K_3M\mathcal{A}_0\mathcal{A}_2+6K_2\mathcal{A}_0^2\mathcal{A}_1^2+\frac{4}{3}\mathcal{A}_2p\mathcal{A}_0+\frac{14}{3}\mathcal{A}_2^2r-K_3M\mathcal{A}_1^2+\frac{4}{3}\mathcal{A}_1^2p=0,$$
$$\frac{1}{3}\mathcal{A}_1p\mathcal{A}_0+\frac{14}{3}\mathcal{A}_2r\mathcal{A}_1-2K_3M\mathcal{A}_0\mathcal{A}_1+4K_2\mathcal{A}_0^3\mathcal{A}_1=0,$$
$$\frac{2}{3}\mathcal{A}_2r\mathcal{A}_0+\mathcal{A}_1^2r+K_2\mathcal{A}_0^4-K_3M\mathcal{A}_0^2=0.$$

Simplifying the above equations, the following expressions are determined:

$$a_0=\sqrt{\frac{5K_3M}{4K_2}},a_1=0,a_2=-\frac{5q}{3\sqrt{5K_2K_3M}},p=p,q=q,r=\frac{16p^2}{25q},s=\frac{15q^2}{64p}.$$

In the influential work in Refs. [26, 33], a new mapping method was developed for solving differential equations, based on constructing exact solutions via transformation methods that rely on certain constraint conditions—specifically, parameters denoted by r and s. Their approach has proven highly effective in generating diverse classes of exact solutions for nonlinear evolution equations (NLEEs) with polynomial nonlinearities. These constraint conditions are central to enabling the solution process and serve as a foundation for classifying and generating solution families.

In our investigation, we apply this framework to a class of nonlinear differential equations exhibiting *non-polynomial* nonlinearities. Surprisingly, it is observed that the classical constraint conditions r and s proposed in Refs. [26, 33] are insufficient to generate exact solutions in this context. That is, while the method yields fruitful results for polynomial forms, it fails to resolve or reduce the equations into a tractable form when the nonlinearities are non-polynomial in nature. Consequently, we establish *new conditions* on the parameters, adapted specifically to the structure of non-polynomial nonlinearities, and thereby successfully derive exact solutions. To illustrate this, Eq. (5.3) can then be converted along with the determined constrains conditions r and s to

$$\left(\frac{d\Psi}{d\xi}\right)^2 = p\Psi^2 + \frac{1}{2}q\Psi^4 + \frac{5q^2}{64p}\Psi^6 + \frac{16p^2}{25q}. \tag{5.4}$$

Motivated by the rational structure of the right-hand side, we propose the following hyperbolic ansatz:

$$\Psi(\xi) = \sqrt{\frac{\alpha\tanh^2(k\xi)}{1+\beta\tanh^2(k\xi)}}, \tag{5.5}$$

or alternatively,

$$\Psi(\xi) = \sqrt{\frac{\alpha\tan^2(k\xi)}{1+\beta\tan^2(k\xi)}}, \tag{5.6}$$

where α, β, k are constants to be determined. Introducing $T = \tanh(k\xi)$, the squared form becomes:

$$\Psi^2 = \frac{\alpha T^2}{1+\beta T^2},$$

which leads to:

$$\left(\frac{d\Psi}{d\xi}\right)^2 = \alpha k^2 \cdot \frac{(1-T^2)^2}{(1+\beta T^2)^3}. \tag{5.7}$$

Expanding the right-hand side of Eq. (5.4) using the ansatz yields:

$$\left(\frac{d\Psi}{d\xi}\right)^2 = \frac{1}{(1+\beta T^2)^3}\left[p\alpha T^2(1+\beta T^2)^2 + \frac{1}{2}q\alpha^2 T^4(1+\beta T^2) + \frac{5q^2}{64p}\alpha^3 T^6 + \frac{16p^2}{25q}(1+\beta T^2)^3\right]. \tag{5.8}$$

By collecting like powers of T from Eqs. (5.7) and (5.8), we compare both sides term by term:

$$\begin{aligned}
&\text{Coefficient of } T^0: \quad \alpha k^2 = \frac{16p^2}{25q},\\
&\text{Coefficient of } T^2: \quad -2\alpha k^2 = p\alpha + \frac{48p^2}{25q}\beta,\\
&\text{Coefficient of } T^4: \quad \alpha k^2 = 2p\alpha\beta + \frac{1}{2}q\alpha^2 + \frac{48p^2}{25q}\beta^2,\\
&\text{Coefficient of } T^6: \quad 0 = p\alpha\beta^2 + \frac{1}{2}q\alpha^2\beta + \frac{5q^2}{64p}\alpha^3 + \frac{16p^2}{25q}\beta^3.
\end{aligned}$$

Solving the resulting algebraic system yields the following via Maple 18 manipulation software:

$$k = \pm\sqrt{-\frac{p}{5}}, \quad \alpha = -\frac{16}{5}\cdot\frac{p}{q}, \quad \beta = 1,$$

Similarly, the following values for k, α and β are determined by considering the alternative soluton:

$$k = \pm\sqrt{\frac{p}{5}}, \quad \alpha = \frac{16}{5}\cdot\frac{p}{q}, \quad \beta = -1.$$

Hence the solution of the considered model equation as in Eq. (1.1) with $a = 0$ and without forced-damped term as

$$V(x,y,z,t) = \left(\sqrt{\frac{5K_3M}{4K_2}} + \frac{16p}{3\sqrt{5K_2K_3M}}\cdot\frac{\tanh^2\left(\sqrt{-\frac{p}{5}}\,\xi\right)}{1+\tanh^2\left(\sqrt{-\frac{p}{5}}\,\xi\right)}\right)^4, \quad p<0, \tag{5.9}$$

and

$$V(x,y,z,t) = \left(\sqrt{\frac{5K_3M}{4K_2}} - \frac{16p}{3\sqrt{5K_2K_3M}}\cdot\frac{\tan^2\left(\sqrt{\frac{p}{5}}\,\xi\right)}{1-\tan^2\left(\sqrt{\frac{p}{5}}\,\xi\right)}\right)^4, \quad p>0. \tag{5.10}$$

where $\xi = lx + my + nz - Mt$. This solution strategy demonstrates that while the original method in Refs. [26, 33] operates effectively under polynomial constraints, its generalization to non-polynomial structures requires novel constraint conditions. The values of α, β, k obtained here represent such a modification, enabling exact solution derivation for classes of nonlinear ODEs previously inaccessible under the standard approach. Even, the JEFM is also not applicable to determine the solutions with this conditions. This constitutes the primary novelty of our contribution: *extending the mapping method to equations with non-polynomial nonlinearities by deriving consistent constraint conditions compatible with the ansatz form.*

Figure 9 presents six novel families of non-polynomial nonlinear wave structures, with analytically derived amplitude variations reported here for the first time. These solutions, obtained from a fourth-power expression involving non-polynomial transformations of hyperbolic tangent and tangent functions, display remarkably diverse spatial behaviors under different parameter sets (p, σ, δ) and obliqueness angle θ. The governing formulation incorporates obliqueness through the effective dispersion parameter $D(\theta)$ and admits both focusing $(p > 0)$ and defocusing $(p < 0)$ regimes. The amplitude of wave propagation, along with its sharpness and degree of localization, is shown to be highly sensitive to the sign and magnitude of p, as well as the obliqueness θ, thereby confirming the rich and tunable solution space. The resulting structures include smooth dark-type profiles, sharply peaked solitons, broad nonlinear dips, and hybrid localized formations, each modulated by parameter variations. Although one can also generate a collection of waveforms by displaying $V(x, y)$, or $V(x, z)$ or $V(y, z)$(while fixing the third spatial variable), this has been omitted here for simplicity. The ability to visualize these exotic waveforms in 3D across obliqueness provides deeper insight into the geometric tunability and directional sensitivity of the solutions. Since these expressions deviate from conventional polynomial nonlinearities, the resulting profiles constitute a significant extension of classical soliton theory, opening avenues for further exploration in systems with higher-order or fractional-gradient effects, and reinforcing both the originality and theoretical depth of the present work.

6. Conclusion

This study presented a comprehensive analytical and numerical exploration of a generalized ZK equation, incorporating mixed nonlinearities, anisotropic dispersion, damping, and external forcing to model obliquely propagating nonlinear waves.

The main findings reveal the profound impact of mixed polynomial and root-type nonlinearities on the system dynamics. Phase portrait analysis demonstrates that pure polynomial nonlinearity yields symmetric phase spaces with homoclinic orbits, while root-type nonlinearity introduces asymmetry and shifts equilibria, indicating wave softening/hardening. The interplay of both nonlinearities, especially under external forcing, leads to complex dynamics, including transitions from regular orbits to weak and fully developed chaos, corresponding to modulational instabilities and wave turbulence. Using a traveling wave reduction, the PDE was transformed into a second-order ODE. Melnikov's method confirmed the existence of transverse homoclinic intersections, revealing the onset of deterministic chaos under suitable conditions—an advancement rarely applied to ZK-type systems with external forcing. Analytically, we extended the new mapping method by deriving new constraint conditions to obtain exact solutions for non-polynomial nonlinearities, which was previously unattainable. A rich spectrum of coherent structures—including bright/dark

solitons and super-nonlinear periodic waves constructed from Jacobi elliptic functions—is systematically classified. These wave morphologies are highly tunable via the elliptic modulus, nonlinear parameters, dispersion coefficients, and the obliqueness angle, which modulates the effective dispersion. Additional Jacobi elliptic solutions were derived for the quadratic case, covering a broad class of waveforms from periodic to solitary profiles. Simulations demonstrated diverse wave regimes, including smooth solitons, periodic patterns, and hybrid localized structures, strongly influenced by obliqueness angle and elliptic modulus. Notably, novel non-polynomial 3D structures were visualized for the first time. Overall, the system exhibits three principal behaviors: integrable-like solitary waves, weak chaos near resonance, and broadband turbulence. These are validated through exact analysis and numerical phase portraits.

This work opens several promising avenues for future research. The extended mapping method could be applied to other nonlinear systems with fractional or higher-order non-polynomial terms. Investigating the stability analysis of the obtained solutions using linear perturbation methods would provide crucial insights into their physical realizability. Furthermore, extending the model to include higher-dimensional effects or quantum corrections could reveal additional rich dynamics relevant to advanced plasma and fluid applications. The study advances ZK theory by introducing new analytical tools, identifying chaotic regimes, and visualizing rich nonlinear wave structures in complex environments, providing a comprehensive framework for understanding complex wave interactions in obliquely propagating plasmas or fluids.

Acknowledgment

The authors would like to thank all members of the Mathematical Physics Research Group, led by Prof. M. G. Hafez, Department of Mathematics, Chittagong University of Engineering and Technology, Bangladesh, for their valuable support and discussions. The authors received no specific funding for this work.

References

[1] S. Akter and M. G. Hafez, *Collisional positron acoustic soliton and double layer in an unmagnetized plasma having multi-species*, Sci. Rep., *12* (2022), 6453.

[2] S. Akter and M. G. Hafez, *Head-on collision between two counter-propagating electron acoustic soliton and double layer in an unmagnetized plasma*, AIP Adv., *13* (2023), 015005.

[3] S. Akther and M. G. Hafez, *Lump soliton, and overtaking collision between lump and single as well as double solitons in an unmagnetized collisionless relativistic plasma*, Alexandria Eng. J., *122*(5–6) (2025), 520.

[4] S. Akther and M. G. Hafez, *KP, MKP and G-KP soliton and overtaking collision among multi-soliton propagation in an unmagnetized (2 + 1)-dimensional collisionless plasma environment*, Discover Space, *129* (2025), 11.

[5] M.N. Alam and C. Tunç, *Constructions of the optical solitons and other solitons to the conformable fractional Zakharov–Kuznetsov equation with power law nonlinearity*, J. Taibah Univ. Sci., *14*(1) (2019), 94–100.

[6] M. Asadullah, A. Javid, N. Raza, et al., *Exploring the (3+1)-dimensional Korteweg–de Vries and Calogero–Bogoyavlenskii–Schiff combined model: travelling waves, bifurcation analysis, quasi-periodic structures and sensitivity analysis*, Nonlinear Dyn., (2025).

[7] S. Barua, M. G. Hafez, and M. O. Rahman, *Dynamics of ion-acoustic soliton propagation near the super-critical values in relativistic magnetized plasmas*, IEEE Trans. Plasma Sci., *53*(5) (2025), 880–892.

[8] L. A. Dawod, M. Lakestani, and J. Manafian, *Breather wave solutions for the (3+1)-D generalized shallow water wave equation with variable coefficients*, Qual. Theory Dyn. Syst., *22*(1) (2023), 127.

[9] S. Disca and V. Coscia, *Melnikov method for a class of generalized Ziegler pendulums*, Mathematics, *13* (2025), 1267.

[10] M. Eslami and H. Rezazadeh, *The first integral method for Wu–Zhang system with conformable time-fractional derivative*, Calcolo, *53*(3) (2015), 255–269.

[11] L. Fu and H. Yang, *An application of (3+1)-dimensional time–space fractional ZK model to analyze the complex dust acoustic waves*, Complexity, *2019*(1) (2019), 2806724.

[12] H. Günerhan, *Analytical solutions of one-dimensional convection–diffusion problems*, Turk. J. Anal. Number Theory, *6*(6) (2019), 152–154.

[13] W. Hamali, J. Manafian, M. Lakestani, and A. Bekir, *Optical solitons of M-fractional nonlinear Schrödinger's complex hyperbolic model by generalized Kudryashov method*, Opt. Quantum Electron., *56*(1) (2023), 1–18.
[14] M. G. Hafez, S. A. Iqbal, Asaduzzaman, and Z. Hammouch, *Dynamical behaviors and oblique resonant nonlinear waves with dual-power law nonlinearity and fractional temporal evolution*, Discrete Contin. Dyn. Syst. Ser. S, *24* (2021), 2245–2260.
[15] S. A. Iqbal, M. G. Hafez, and M. F. Uddin, *Bifurcation features, chaos, and coherent structures for one-dimensional nonlinear electrical transmission line*, Comput. Appl. Math., *41* (2022), 50.
[16] J. Kuang, S. Tan, K. Arichandran, and A. Y. T. Leung, *Chaotic attitude motion of gyrostat satellite via Melnikov method*, Int. J. Bifurc. Chaos, *11* (2001), 1233–1260.
[17] M. Y. Khattak, W. Masood, R. Jahangir, and M. Siddiq, *Interaction of ion acoustic solitons for Zakharov–Kuznetsov equation in relativistically degenerate quantum magnetoplasmas*, Waves Random Complex Media, *34*(4) (2021), 2750–2766.
[18] M. Lakestani, J. Manafian, A. R. Najafizadeh, and M. Partohaghighi, *Some new soliton solutions for the nonlinear fifth-order integrable equations*, Comput. Methods Differ. Equ., *10*(2) (2022), 445-460.
[19] R. J. LeVeque, *Finite Volume Methods for Hyperbolic Problems*, Cambridge University Press, Cambridge, (2002).
[20] S. Liu, Z. Fu, S. Liu, Q. Zhao, *Jacobi elliptic function expansion method and periodic wave solutions of nonlinear wave equations*, Phys. Lett. A, *289* (2001), 69–74.
[21] J. Liu, M. Nadeem, *Analysis of the dynamical perspective of chaos, Lie symmetry, and soliton solution to the Sharma–Tasso–Olver system*, Nonlinear Dyn., *112* (2024), 3835–3850.
[22] J. Manafian, L. A. Dawood, and M. Lakestani, *New solutions to a generalized fifth-order KdV like equation with prime number via a generalized bilinear differential operator*, Partial Differ. Equ. Appl. Math., *9* (2024), 100600.
[23] V. K. Mel'nikov, *On the stability of a center for time-periodic perturbations*, Tr. Mosk. Mat. Obs., *12* (1963), 3–52.
[24] W. Qiu, J. Zhang, C. Hu, et al., *Nonlinear dynamic analysis of the longitudinal surge oscillations in hydraulic transients of a hydropower system featuring a pipe-shaped air chamber*, Nonlinear Dyn., (2025).
[25] M. O. Rahman, M. G. Hafez, S. Barua, and M. A. Kauser, *Ion acoustic solitons and periodic waves with dynamical features around the supercritical values in relativistic unmagnetized plasmas*, Phys. Scr., *100*(2) (2025), 025201.
[26] H. U. Rehman, A.F. Aljohani, A. Althobaiti, S. Althobaiti, and I. Iqbal, *Diving into plasma physics: dynamical behaviour of nonlinear waves in (3+1)-D extended quantum Zakharov–Kuznetsov equation*, Opt. Quantum Electron., *56* (2024), 1336.
[27] C. Robinson, *Melnikov method for autonomous Hamiltonians*, Contemp. Math., *198* (1996), 45–53.
[28] M. M. Sarkar, S. Barua, and M. G. Hafez, *Ion-acoustic wave propagation with Bohm quantum potential near and at supercritical values in degenerate plasmas*, Phys. Plasmas, *32*(7) (2025), 072703.
[29] C. Shi, Y. He, D. Sheen, and X. Feng, *A difference finite element method for convection–diffusion equations in cylindrical domains*, Int. J. Numer. Anal. Model., *21*(3) (2024), 407–430.
[30] M. F. Uddin, M. G. Hafez, and S. A. Iqbal, *Dynamical plane wave solutions for the Heisenberg model of ferromagnetic spin chains with beta derivative evolution and obliqueness*, Heliyon, *8*(3) (2022), e09199.
[31] Y. Xiao, *Impacts of a general power law on soliton for a (2+1)-dimensional Zakharov–Kuznetsov equation in magnetized quantum plasmas*, Results Phys., *47* (2023), 106340.
[32] E. M. Zayed, K. A. Alurrfi, and R. A. Alshbear, *On application of the new mapping method to magneto-optic waveguides having Kudryashov's law of refractive index*, Optik, *287* (2023), 171072.
[33] X. Zeng and X. Yong, *A new mapping method and its applications to nonlinear partial differential equations*, Phys. Lett. A, *372* (2008), 6602–6608.
[34] Z. Zhao, Y. Liu, Y. Zhang, and J. Pang, *Study on the interaction solution of Zakharov–Kuznetsov equation in quantum plasma*, Therm. Sci., *28*(3A) (2024), 1999–2008.
[35] H. Zhu, J. Manafian, and A. H. Hammadi, *Conservation law, Chupin Liu's theorem and propagation of pulses in optical metamaterials modeled by NLSE with power law nonlinearity*, Sci. Rep., *15*(1) (2025), 21649.